ACS Catalysis

Research Article

pubs.acs.org/acscatalysis

Iridium- and Platinum-Free Ring Opening of Indan

Jing Shen and Natalia Semagina*

Department of Chemical and Materials Engineering, University of Alberta, 9107-116 St., Edmonton, Alberta T6G 2V4, Canada

Supporting Information

ABSTRACT: A 3- and 2-fold increase in selectivities toward 2-ethyltoluene and *n*-propylbenzene, respectively, in indan ring opening (RO) was achieved by introducing palladium to the ruthenium catalyst. The product selectivities for the Ru−Pd system with the 4:1 molar ratio were the same as those for monometallic iridium, known for its outstanding single cleavage selectivity; the lights formation was suppressed as compared with the monometallic platinum catalyst. A further increase in the Pd amount did not result in the selectivity improvement and brought down the activity to the low level of Pd. The bimetallic catalysts were synthesized in the presence of poly-(vinylpyrrolidone). The bimetallic systems revealed sintering resistance up to 400 °C, as compared with their monoforms. The indan RO activity was maximized after precalcination at 200 °C. The suggested nanoparticles' bimetallicity was consistent with the results of CO-TPD, CO−DRIFTS, thermal stability tests, and a chemical probe reaction (olefin hydrogenation, in which only Pd is active). The Pd−Ru system is envisioned as a viable alternative to monometallic Ir for RO.

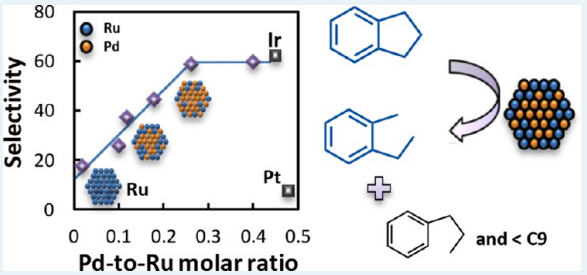

KEYWORDS: *indan, palladium, ruthenium, PVP, nanoparticles, bimetallic, core−shell, synergism*

INTRODUCTION

Ring opening (RO) of naphthenic rings, when only one C−C bond is cleaved, maintaining the same number of carbon atoms,[1] is an attractive reaction for improving fuel quality. Although RO does not necessarily result in the cetane number improvement because of the formation of highly branched products via cleavage of unsubstituted C−C bonds (as opposed to the RO at the substituted positions),[2] it offers other potential benefits to refineries, such as volume increase, improvement of cloud point, and decrease of the polynuclear aromatics content. Catalytic metal function is paramount for RO, as an acid function, necessary for a preliminary six-ring contraction of aromatics to the five-ring, leads to excessive cracking.[3−11] Metal catalysts offer three RO mechanisms: dicarbene, π-adsorbed olefin, and metallocyclobutane reaction paths.[12] The dicarbene path results in the cleavage of unsubstituted secondary-secondary C−C bonds, producing highly branched isoparaffins, with π-adsorbed olefin and metallocyclobutane pathways, leading to C−C opening at the substituted positions.

The most active RO catalyst is iridium, which, in most examples, works through the dicarbene mechanism.[4,13,14] Platinum has very low activity, but in the RO product distribution, it may be more selective toward unbranched products via π-adsorbed olefin or metallocyclobutane paths. Ir-based systems are probably the most studied and reported RO catalysts, with the bimetallic Ir−Pt catalyst being used in refineries as one of the naphtha reforming catalysts.[15] The search for less expensive alternatives driven by the oil industry is getting more complicated, as the fuel regulations have become more stringent with the simultaneous decrease in the quality of crude oil. Iridium, which is one of the rarest elements on Earth, is sought to be replaced by a catalyst with high hydrogenolysis activity to maintain high RO yields and to prevent catalyst coking,[16] while the role of platinum in forming products with higher cetane numbers and its hydrogenation ability should not be lost, either.

The objective of our work was to develop less expensive iridium- and platinum-free alternatives for RO. Only metal function is targeted in the current work. The search for an Ir alternative is complicated by its highest known RO activity.[1] A recent density functional theory (DFT) study revealed that the activation barrier for MCP RO increases in the order of Rh < Ir ≪ Pt < Pd, which is consistent with experimentally observed activities.[17] Rh, Re, Ru, and Ni show a similar RO mechanism as Ir (i.e., rupture of unsubstituted C−C bonds), but they are found to be less selective than Ir because of the extensive secondary cracking of the primary C_6-alkane RO products to C_1−C_5 paraffins, especially in the case of Ru.[1,18] Catalytic properties are also greatly affected by the reactant nature.[3] In pentylcyclopentane RO, the RO selectivities follow the trend Ir (92%) > Rh (87%) > Ru(82%) > Pt(68%).[1] In methylcyclohexane RO, the trend is Ir (87%) ≫ Pt, Ni and Ru (4−5%),[1] but in the C_7-alkane product distribution, *n*-hexane is produced in higher amounts by Ru (13%) than by Ir (5%). This indicates that Ru might be a valid alternative to Ir, and it could even outperform Ir in terms of cetane number improvement in real complex feeds, as compared with simple model compounds.

A feasible way to bring up the selectivity of Ru toward single-cleavage products, at least to the level of Ir, is to add a second component, creating a bimetallic catalyst.[19] A variety of

Received: July 10, 2013
Revised: December 6, 2013
Published: December 10, 2013

 © 2013 American Chemical Society

bimetallic catalysts were reported for RO.[18,20−26] Among them, a Pt−Rh bimetallic catalyst allowed for the increasing RO activity and selectivity, which were similar to those of Ir catalysts,[20] but the cost of Rh sets limitations on the catalyst exploitation. The addition of Ru to Pt improved Pt RO activity only when there was a high Ru portion in the bimetallic system; the bimetallic Pt−Ru catalyst favored deep hydrogenolysis compared with the catalytic behavior of the monometallic Pt catalyst, regardless of the Ru content.[18]

In selecting the second metal for the alternatives to the currently used Pt−Ir system, it is paramount to keep the Pt-like mechanism of RO via a flat-lying mode.[1,27] Only Pd follows a similar mechanism.[28] It was not studied as frequently as Pt in RO because of its very low activity.[17,29] The substitution of Pt by Pd in Ir-based bimetallic RO catalysts was addressed in some recent works. In our study of indan RO, Pd was shown to serve only as a dispersing agent to Ir, without contributing to its intrinsic activity or selectivity, as long as an ensemble of two Ir atoms required for the dicarbene path was not destroyed by Pd addition, resulting in activity loss.[24] Another study included tetralin hydroconversion in the presence of ppm amounts of H_2S and revealed that the catalytic activity increased with Pd content, while the selectivity to RO/contraction products reached the maximum at Ir55−Pd55 composition.[25]

Thus, a Ru−Pd system may be envisioned as a prominent alternative to the Ir−Pt system, as soon as the high hydrogenolysis activity of Ru, resulting in lower selectivity as compared with Ir, can be reduced by Pd addition. Notably, the d-level occupancy of Ir is in between the levels for Ru and Pd; thus, it seems feasible to create a Ru−Pd bimetallic system with a similar surface free energy as Ir. Both Ru and Pd have close atomic radii, and the bimetallic crystal structure may be predicted to change from the f.c.c. structure of Pd to the h.c.p. structure of Ru with increasing Ru content, as shown for Pt−Ru systems.[30] We recently addressed the probability of using some Ru−Pd catalysts in indan RO,[31] which showed that their activity and selectivity decreased as compared with their monometallic counterparts and were lower than those of Ir, but the used bimetallic nanoparticle sizes were significantly larger than those of monometallic ones, and the applied synthetic methods were different. The previously applied procedure to prepare Ru-rich nanoparticles resulted in Pd abundance in the nanoparticle outer shell, as confirmed by ion scattering spectroscopy, with Pd being responsible for poor activity. Still, motivated by the system potential, we extended our quest to the mono- and bimetallic nanoparticles of similar size of ∼2−3 nm, but with wide ranges of Pd-to-Ru ratios and various loci of the two atom types in a nanoparticle. The modified synthetic techniques allowed us to enrich the nanoparticle shell with Ru atoms for some catalysts. It should be noted that the used abbreviations only reflect the molar composition of final catalysts (such as Ru4Pd1) or the mode of a catalyst preparation (such as Pd(core)Ru(shell)), and they should not be considered as a phase composition or a real structure of the nanoparticle. As will be shown below, the developed nanoparticle synthetic techniques yielded a Ru−Pd catalyst with as high selectivity as Ir in a model RO reaction of indan (Scheme 1) and suppressed lights formation as compared with Pt.

EXPERIMENTAL SECTION

Materials. Ruthenium(III) nitrosylnitrate ($Ru(NO)(NO_3)_3$, Alfa Aesar), palladium(II) chloride solution ($PdCl_2$, 5% w/v, Acros), hydrogen hexachloroiridate(IV) hydrate (H_2IrCl_6, 99.98%, Sigma-Aldrich), chloroplatinic acid solution (H_2PtCl_6, 8 wt % in H_2O, Sigma-Aldrich), poly-(vinylpyrrolidone) (PVP) (MW: 40,000, Sigma-Aldrich), reagent alcohol (ethanol, 95 vol. %, Fisher Scientific), ethylene glycol (EG, 99.8%, Sigma-Aldrich), gamma-aluminum oxide (γ-Al_2O_3, 150 mesh 58 Å pore size, Sigma-Aldrich), acetone (99.7%, Fisher Scientific), and 2-methyl-3-buten-2-ol (MBE, 97%, Acros Organics) were used as received. Argon, hydrogen, 10% hydrogen in helium, 10% oxygen in argon, and 3% carbon monoxide in helium of ultrahigh purity 5.0 were purchased from Praxair. Milli-Q water was used throughout the work.

Scheme 1. Reaction Scheme for Low-Pressure Indan RO on a Metal Function;[37] Reproduced with Permission from Ref 37. Copyright 2006 Elsevier

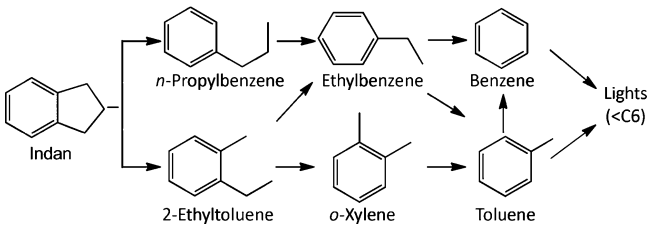

Catalyst Preparation and Pretreatment. All catalysts were prepared by growing 2−3 nm nanoparticles in a colloidal dispersion in the presence of PVP, followed by precipitation on γ-Al_2O_3 with 5.8 nm pores and high-temperature PVP removal. As opposed to our previous work, in which large nanoparticles were obtained with the PVP/metal(s) molar ratio of 10/1,[31] in this work, the ratio was kept at 20 (unless indicated otherwise), and the synthetic procedures were modified, which allowed for us to produce ∼2−3 nm nanoparticles with various loci of the two atom types in a nanoparticle.

A summary of the prepared catalysts is presented in Table 1. Monometallic Pd nanoparticles were synthesized by Teranishi and Miyake's one-step alcohol (ethanol/water system) reduction method[32] with some modifications. A mixture containing 0.712 mL (0.2 mmol) of 5% w/v $PdCl_2$ aqueous solution, 170 mL of ethanol/water ([ethanol] = 41 vol.%), and 0.444 g of PVP (MW 40,000) was stirred and refluxed in a 500 mL 3-neck round-bottom flask for 3 h under air. The PVP-stabilized monometallic Ru, Ir, and Pt nanoparticles were prepared using the ethylene glycol (EG) reduction method.[33,34] At room temperature, 0.2 mmol of metal precursor salt ($Ru(NO)(NO_3)_3$, H_2IrCl_2, or H_2PtCl_6) and 0.444 g of PVP (MW 40,000) were well dissolved in 200 mL of EG in a 500 mL single-neck round-bottom flask. The reduction temperature was increased from room temperature to the reflux point of EG (198 °C), and then it was maintained at 198 °C for 3 h. After reactions, transparent dark-brown macroscopically homogeneous colloidal dispersions of monometallic Ru, Pd, Ir, and Pt nanoparticles were obtained without any precipitate.

In this study, three different synthesis techniques were applied to produce Ru−Pd bimetallic nanoparticles: (1) to obtain catalysts with high Ru-to-Pd molar ratio, a simultaneous reduction of both Ru and Pd precursors was applied using the synthetic procedure for monometallic Ru nanoparticles. Three different metal molar ratios were synthesized: Ru10Pd1, Ru8Pd1, and Ru6Pd1 (Ru/Pd molar ratios = 10/1, 8/1, and 6/1, respectively). The total amount of Ru and Pd precursors in each synthesis was 0.2 mmol, while all other experimental conditions were kept the same. (2). To obtain catalysts with

dx.doi.org/10.1021/cs400986v | ACS Catal. 2014, 4, 268−279

Table 1. Summary of the Synthesized Nanoparticles and γ-Al_2O_3-Supported Catalysts

metal precursor(s)	reducing agent[a]	synthesized nanoparticles[b]	size distribution,[d] nm	metal loading in supported catalysts, wt %
Pd^{2+}	Et/H_2O	Pd	2.0 ± 0.5	0.231
	EG	Pd	~7	not used for catalysis
Ru^{3+}	Et/H_2O	no reduction		N/A
	EG	Ru	2.0 ± 0.3	0.300
high molar ratio of Pd^{2+}/Ru^{3+}	Et/H_2O (Scheme 2)	Ru4Pd1	2.2 ± 0.5	Ru: 0.166, Pd: 0.046
		Ru2Pd1	2.6 ± 0.6	Ru: 0.154, Pd: 0.065
		Ru1Pd1	3.1 ± 0.7	Ru: 0.111, Pd: 0.090
		Ru1Pd2	2.8 ± 0.5	Ru: 0.082, Pd: 0.143
	EG[c]	(Ru4Pd1)[c]	2.9 ± 0.6[c]	
		(Ru1Pd1)[c]	3.6 ± 1.2[c]	N/A[c]
		(Ru1Pd2)[c]	5.3 ± 0.9[c]	
high molar ratio of Ru^{3+}/Pd^{2+}	EG	Ru10Pd1	2.1 ± 0.4	Ru: 0.0267, Pd: 0.028
		Ru8Pd1	2.0 ± 0.3	Ru: 0.275, Pd: 0.034
		Ru6Pd1	2.0 ± 0.3	Ru: 0.206, Pd: 0.039
Pd° (2 nm) and Ru^{3+}	Et/H_2O (Scheme 3)	Pd(c)Ru(s), Ru/Pd = 1.6	2.3 ± 0.7	Ru: 0.140, Pd: 0.095
Ir	EG	Ir	1.7 ± 0.3	0.173
Pt	EG	Pt	3.2 ± 0.4	0.205

[a]Et, ethanol; EG, ethylene glycol. [b]Numbers in the catalyst notation correspond to the rounded molar ratio of the two metals in the supported catalysts, as determined by NAA. [c]These catalysts were synthesized and reported for the same catalytic reaction in our previous work.[31] [d]TEM images and size distribution histograms for the Pd–Ru materials are presented in Supporting Information.

lower Ru-to-Pd molar ratio but Ru-enriched surfaces, we used a modified general synthetic procedure for the synthesis of Ru–Pt nanoparticles, proposed by Liu et al.[35] (Scheme 2). The

Scheme 2. Synthesis of Ru4Pd1, Ru2Pd1, Ru1Pd1, and Ru1Pd2 Catalysts with Ru-Enriched Shells

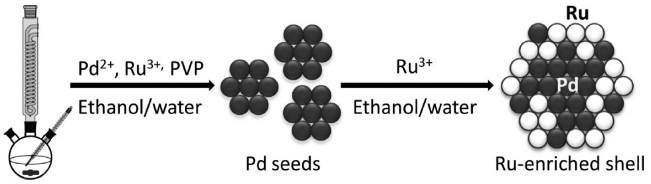

experimental conditions followed the preparation method for monometallic Pd nanoparticles in an ethanol/water system, with 0.2 mmol of Ru and Pd in each reaction. A series of Ru–Pd nanoparticles with different compositions were prepared by varying Ru-to-Pd molar ratios: Ru4Pd1, Ru2Pd1, Ru1Pd1, and Ru1Pd2. 3). To obtain the Pd(core)-Ru(shell) nanoparticles (Scheme 3), Teranishi and Miyake's stepwise growth reaction method was applied.[32] A 42.5 mL portion of colloidal solution containing 0.05 mmol of PVP-stabilized Pd core nanoparticles were prepared using the synthesis method of monometallic Pd nanoparticles. A 0.032 g portion of $Ru(NO)(NO_3)_3$ precursor (0.1 mmol) and the presynthesized Pd core colloidal solution were dissolved in 170 mL of ethanol/water ([ethanol] = 41 vol. %) at room temperature. This mixture was then heated up to its reflux point. During the shell preparation step, no more fresh PVP was added. A dark brown macroscopically homogeneous colloidal dispersion of Pd(c)Ru(s) nanoparticles was obtained after refluxing for 3 h without any precipitate.

Nanocatalyst support, γ-Al_2O_3, was dried in an oven at 200 °C for 12 h. PVP-stabilized monometallic Ru, Ir, and Pt and bimetallic Ru–Pd nanoparticles prepared in EG were precipitated with acetone and deposited on γ-Al_2O_3 by wet impregnation. PVP-stabilized monometallic Pd and bimetallic Ru–Pd nanoparticles prepared in an ethanol/water system were deposited on γ-Al_2O_3 by incipient impregnation. Finally,

Scheme 3. Formation of Ru–Pd Bimetallic Nanoparticles with Pd (Core)–Ru (Shell) Structure

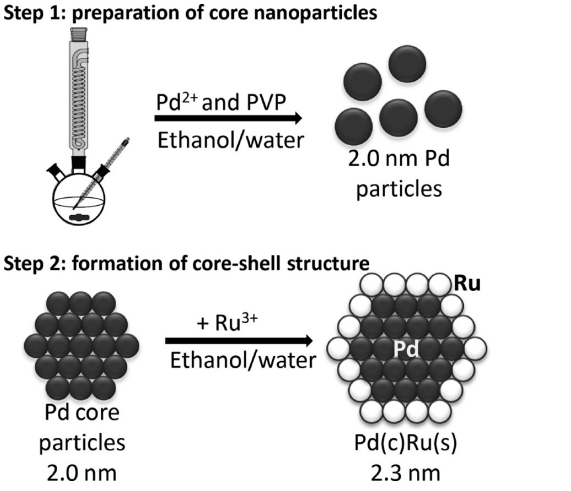

all catalysts were dried in a fume hood. The target loading was 0.3 wt %. Table 1 shows metal loadings for the synthesized supported catalysts determined by neutron activation analysis.

Catalyst Characterization. Transmission electron microscopy (TEM), neutron activation analysis (NAA), and X-ray photoelectron spectroscopy of as-prepared metal nanoparticles and/or supported catalysts were performed as described earlier.[31] For the TEM, 100–200 particles per sample were counted.

Temperature Programmed Reduction (TPR). TPR experiments of supported catalysts were performed with H_2/Ar gas mixture using an AutoChem 2950HP instrument (Micromeritics, U.S.A.) equipped with a thermal conductivity detector (TCD). To eliminate any effects arising from PVP removal, a series of oxidation–reduction–oxidation–reduction were performed, and the reported results refer to the final reduction step. Prior to the analysis, the catalysts with as-deposited nanoparticles were calcined at 200 °C in air for 2 h; 0.5 g of precalcined catalysts were loaded in a quartz reactor.

dx.doi.org/10.1021/cs400986v | ACS Catal. 2014, 4, 268–279

The precalcined catalysts were reduced in a flow of 10% H_2/Ar (50 mL/min) at 375 °C for 1 h. These conditions simulate the pretreatment procedure before the RO reactions. After the calcination-reduction pretreatment, the samples were flashed with inert (He) for 30 min at 375 °C and cooled down to ambient temperature under inert. The catalysts were then heated in a flow of 10% O_2/He gas mixture at a linear rate of 10 °C/min from room temperature to 400 °C (to make sure that all PVP was removed as its decomposition temperature is 350 °C) and then flashed with inert (Ar) for 30 min at 400 °C and cooled down to room temperature in Ar. This oxidation procedure was then followed by a TPR analysis from room temperature to 400 °C (i.e., heating in 10% H_2/Ar gas stream at 10 °C/min). The TCD signals for TPR profiles are reported as inverted signals; thus, positive peaks refer to the consumption of hydrogen (due to relative thermal conductivities of Ar and H_2).

CO Chemisorption. The catalyst samples were calcined at five different temperatures: 200, 250, 300, 350, and 400 °C, followed by the reduction 375 °C as described above in TPR sample preparation. Dynamic CO pulse chemisorption analyses were performed by dosing 3% CO/He gas mixture at room temperature with an AutoChem 2950HP instrument. The volumetric flow rates of CO/He loop gas and He carrier gas were 10 mL/min and 50 mL/min, respectively. The amount of catalyst varied from 0.2 to 2 g to obtain equally sized TCD peaks within 10 doses. CO uptake per gram of pure support (γ-Al_2O_3) was also evaluated using 2 g of alumina, which was subtracted from the values for the supported catalysts.

Temperature Programmed Desorption of CO (CO-TPD). PVP-stabilized nanocatalysts were calcined at 350 °C for 1 h to efficiently remove surface polymers, according to the CO-chemisorption results. The precalcined catalyst (0.75−0.80 g) was packed in the quartz reactor and reduced in 10% H_2/Ar at 375 °C for 1 h. The reduced sample was outgassed at 375 °C under Ar for 30 min and then cooled down to room temperature in Ar. Then, 3% CO/He was passed through the sample for 30 min with a flow rate of 50 mL/min. The physically adsorbed CO was removed by flashing the sample with He for 30 min. The sample was then heated up under He flow (10 mL/min) from room temperature to 400 °C with a ramping rate of 10 °C/min, while the TCD signals of CO desorption were recorded as a function of temperature. Two controlled runs were made on the γ-alumina support and a mono-Ru/γ-alumina catalyst without CO treatment. Additionally, CO chemisorption of bare support has proven that the amount of CO adsorbed by γ-alumina is negligible, which is less than 1 mol.% of the CO molecules adsorbed by the supported catalyst. Thus, the observed TCD signals correspond only to desorption of CO molecules from metallic surfaces.

Diffuse Reflectance Infrared Fourier Transform Spectroscopy of the Adsorbed CO (CO−DRIFTS). Diffuse reflectance infrared spectra were obtained using NEXUS 670 FT-IR fitted with a Smart Diffuse Reflectance accessory. The catalysts were prepared with an expected metal loading of 2 wt %. The PVP-stabilized mono- and bimetallic Ru−Pd catalysts were calcined at 200 °C for 1 h to imitate the conditions of pretreatment before the catalytic reaction, reduced in 10% H_2/Ar flow at 375 °C for 30 min, then purged with Ar at 375 °C for 30 min and finally cooled down to room temperature in the inert gas. Then 3% CO/He was passed through the sample for 30 min with a flow rate of 50 mL/min. Finally, the gas phase CO was removed by purging Ar for 30 min. DRIFT spectra were recorded against a KBr standard with 256 scans and a resolution of 4 cm^{-1}. Each sample was measured three times to ensure repeatability. Resolution enhancement and data processing were performed with OMNIC software. The absorption bands were deconvoluted using Origin software.

Chemical Reaction Probe for Surface Pd. To elucidate whether some Pd atoms are present in the outermost layer of bimetallic nanoparticles, a reaction was selected that was catalyzed by Pd and that did not show any conversions on Ru, which was the hydrogenation of 2-methyl-3-buten-2-ol to a corresponding saturated alcohol (Scheme 4).

Scheme 4. Chemical Reaction Probe for Surface Pd Atoms

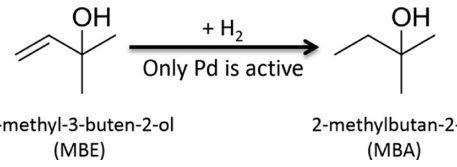

The reactions were carried out in a semibatch stainless steel reactor (300 mL autoclave, Parr Instruments 4560 mini Bench Top Reactor) equipped with a high-temperature fabric heating mantle, a gas buret for the continuous isobaric hydrogen supply, and thermocouple, as described previously.[36] The hydrogenation of MBE was conducted at 40 °C and 0.45 MPa absolute pressure. The reactor was filled with 0.04 M MBE in 200 mL of ethanol and 0.5 g of as-prepared catalyst, flashed with nitrogen, and stirred to reach the reaction temperature. Once the desired reaction temperature was achieved, the reactor was then flashed and pressurized with hydrogen. The stirring speed was 1,200 rpm. The experimental conditions have previously confirmed the absence of mass transfer limitations.[36] During the reaction, hydrogen pressure in the gas buret and the reactor's internal temperature were recorded. At least three catalytic trials were performed for most of the catalysts. The initial reaction rate was considered as the consumption rate of hydrogen; it was calculated from the slope of the hydrogen consumption graph once the hydrogen dissolution had completed.

Low Pressure RO of Indan. Low pressure indan RO (Scheme 1) was performed in a packed bed reactor according to our previous study, with some modifications in the experimental conditions.[31] The PVP-stabilized monometallic Pd, Ru, Ir, and Pt, and bimetallic Ru−Pd catalysts were calcined at 200 °C in an oven under air for 2 h. Catalysts were then reduced in situ at 375 °C under a hydrogen flow (80 mL/min) for 1 h. The precalcined catalyst loading to the reactor corresponds to 4 mg active metal(s), unless stated otherwise. Indan was fed into the catalytic system by bubbling 120 mL/min H_2 through indan at a constant temperature bath at 10 °C. An indan flow rate of $(4.7 \pm 0.6) \times 10^{-6}$ mol/min was confirmed by GC, which was calibrated using a gas cylinder containing indan with a known concentration. A high H_2-to-indan molar ratio, 900−1500 mol_{H2}/mol_{indan}, was used to avoid coke formation. The reactions were performed at an internal temperature of 350 °C and 1 atm pressure. The outgoing stream was analyzed online with a Varian 430-GC-FID every 24 min after the reaction was started. The detailed GC conditions can be found elsewhere.[31] In the previous study, we reported that the RO products are 2-ethyltoluene, *n*-propylbenzene, *o*-xylene, ethylbenzene, toluene, benzene, and lights (mainly methane and ethane), which are in agreement with the results

dx.doi.org/10.1021/cs400986v | ACS Catal. 2014, 4, 268−279

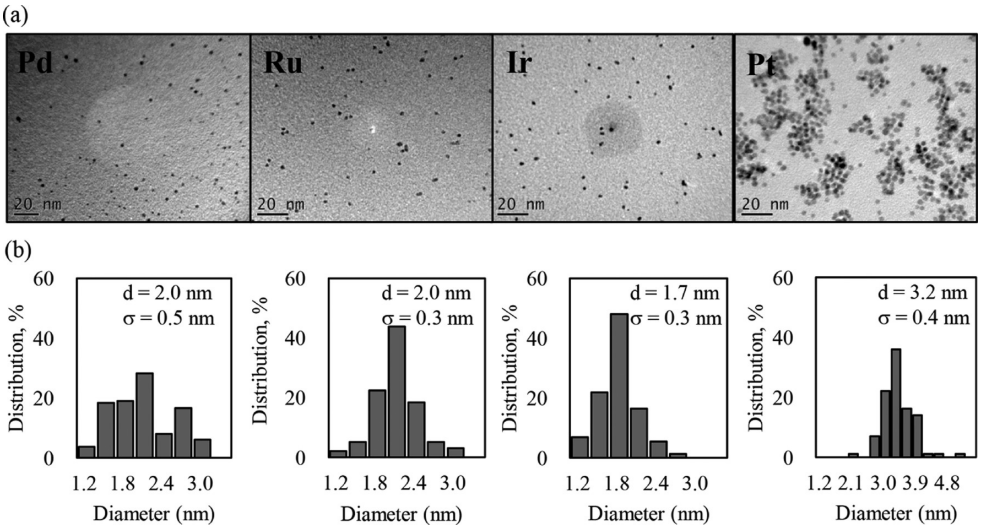

Figure 1. TEM images of PVP-stabilized Pd, Ru, Ir and Pt colloids (a) and corresponding size distribution histograms (b).

published by Nylen et al.[37] The desired RO products are 2-ethyltoluene and *n*-propylbenzene, in which the naphthenic ring has been cleaved only once. Further dealkylation to toluene, benzene, and lights, is undesirable.

A steady state was achieved at 80 min time on stream. Raw GC results were corrected for indan impurities, and all calculations for catalytic performances were based on the corrected GC results. The selectivities are reported on a mass basis as molar selectivity can give a distorted picture of indan utilization, because up to 9 moles of methane may be produced per mole of indan. The GC-FID response factors for 2-ethyltoluene, *n*-propylbenzene, ethyltoluene, and lights were found using calibration cylinders with a known concentration for each component; GC areas for benzene and toluene were calibrated using a bubbler by assuming saturation in H_2. Catalytic properties at 100 min time on stream are reported.

RESULTS AND DISCUSSIONS

Characterization of As-Prepared Nanoparticles. *TEM.* To avoid possible size effects in the catalytic performance of different mono- and bimetallic nanoparticles, our goal was to develop nanoparticles with similar sizes (within 2−3 nm range) as monodispersed as possible. Metal nanoparticle stabilization with PVP is a well-known method,[32,38,39] and we modified the generally known synthetic procedures to ensure the size consistency between the different metals, as the size control was found to be dependent on the metal(s) used.

Table 1 summarizes the synthetic procedures and size of prepared nanoparticles and their metal loading after deposition on γ-Al_2O_3. The TEM images and size distribution histograms of the monometallic particles are shown in Figure 1, and the same for the Pd−Ru materials can be found in the Supporting Information (Figure S1). The numbers in the catalyst notation (such as Ru4Pd1) correspond to the rounded molar ratio of the two metals in the deposited catalysts as determined by NAA. Pd(c)Ru(s) refers to Pd(core)Ru(shell) and is an abbreviation to show a different catalyst preparation method (Ru reduction on the preformed Pd nanoparticles).

The obtained bimetallic nanoparticle sizes with the selected reducing methods are consistent with their intrinsic bimetallic nature. When monometallic Pd is reduced by ethanol (Et), 2 nm nanoparticles are observed, while the reduction by ethylene glycol (EG) produces ∼7 nm particles. Monometallic Ru can be reduced only by EG to 2 nm particles, and no nanoparticle formation was observed in Et. To ensure the reduction, when bimetallic nanoparticles were prepared with high a Ru/Pd molar ratio (Ru10Pd1, Ru8Pd1, and Ru6Pd1), EG was used as a reductant. An average mean diameter of 2.0 ± 0.3 nm was obtained among all the three Ru−Pd bimetallic nanoparticles; if monometallic Pd nanoparticles were present, the 7 nm particles would have been observed. This suggests the bimetallic nature of the nanoparticles, instead of the physical mixtures of 2 and 7 nm particles, corresponding to Ru and Pd, respectively.

However, EG reduction is only an effective method for high Ru content in the Ru−Pd bimetallic system; otherwise, Ru−Pd bimetallic particles reveal not only large particle sizes but also irregularity in particle shapes, and the latter is most likely attributed to the different lattice structures of Pd (f.c.c.) and Ru (h.c.p.). For Pt−Ru systems, the bimetallic crystal structure was found to change from the f.c.c. structure of Pd to the h.c.p. structure of Ru with increasing Ru content.[30] Indeed, in our previous work,[31] when Ru and Pd precursors at a high Pd/Ru ratio were reduced in EG, particles of up to 6 nm diameter were observed (see Table 1), and they did not show promising catalytic activity in the RO reaction. In this work, to gradually increase the Pd fraction in the bimetallic structures and preserve their monodispersity, an ethanol/water reduction method[35] was introduced (Ru4Pd1, Ru2Pd1, Ru1Pd1, and Ru1Pd2 in Table 1), that is, the sequential reduction of Pd and then Ru precursors (Scheme 2). It is well-known that Pd precursors can be easily reduced to Pd metal at a low temperature in alcohol solutions and that the reduced nanoparticles exhibit high monodispersity and a near-spherical shape.[32] Contrary to Pd, the reduction of Ru requires relatively high temperatures; no Ru particles were obtained in low boiling point solvents, such as ethanol/water, which has been examined experimentally (Ru precursor reduction does not occur in ethanol). However, when Pd was present in the Ru^{3+}/ethanol system, Ru precursor was successfully reduced. On average, Ru4Pd1, Ru2Pd1, Ru1Pd1, and Ru1Pd2 prepared by Et-reduction have a mean diameter of 2.7 nm. Larger bimetallic particles, as compared with Pd prepared with the same procedure, are indicative of the reduction and growth of Ru

dx.doi.org/10.1021/cs400986v | ACS Catal. 2014, 4, 268−279

atoms on the surface of Pd seeds, and, thus, the bimetallic nature of the synthesized nanoparticles.

We did not elucidate the mechanism of the bimetallic nanoparticle formation. Autocatalytic surface-growth mechanism has been discussed for the formation of noble-metal clusters, when the aggregation of metal ions to small clusters may occur without reducing electrons; the growing oxidation state of the cluster enhances its electron affinity.[40] This may explain why the Ru precursor could be reduced by ethanol in the presence of palladium: Pd^{2+} is easily reduced by ethanol and forms seeds for the further crystal growth by Ru^{3+} deposition followed by facilitated reduction. The order of the reduction is also in line with the standard electrode potentials: +0.915 eV for Pd^{2+}/Pd and +0.68 eV for Ru^{3+}/Ru. The metal (Pd) with the highest potential is reduced first and forms the seeds. Similarly, Liu et al. observed that if there are metallic seeds available, for example, Pt nanoparticles, the reduction of Ru^{3+} can take place on the surface of the seeds to produce zerovalent Ru metal nanoparticles autocatalytically.[35]

A different 2-step alcohol reduction synthesis for Pd core-Ru shell nanoparticles was used to place Ru atoms only in the nanoparticle shell. Monometallic Pd nanoparticles were synthesized first with an average diameter of 2 nm. Ru precursor was then added to the Pd colloidal dispersion, followed by the reduction of Ru^{3+} and deposition on Pd core particles (Scheme 3). The obtained Pd(c)Ru(s) nanoparticles have an average mean diameter of 2.3 nm (Table 1 and Figure S1 in Supporting Information). The nanoparticles increase in size with the addition of Ru precursors, indicating that Pd nanoparticles in the solution serve as nuclei for larger core−shell particles.[32] According to the metal crystal statistics,[41] the 2 nm Pd nanoparticles correspond to an f.c.c. cuboctahedron with 3 atoms on the crystal edge, and to build one more full shell of Ru atoms (which have a similar diameter to Pd), the 2-to-1 Ru-to-Pd molar ratio is required. The ratio determined by NAA of the deposited Pd(c)Ru(s) nanoparticles is 1.6-to-1, which implies that all Ru atoms are mostly likely 100% dispersed on the Pd core nanoparticle. The formation of monometallic Ru particles is unlikely, as no Ru nanoparticles were observed when the Ru precursor alone was treated in ethanol/water.

Chemical Probe Reaction. To further confirm the bimetallic structure of the as-prepared nanoparticles, they were deposited on γ-Al_2O_3 and used without any further pretreatment in a chemical probe reaction, which was the three-phase hydrogenation of 2-methyl-3-buten-2-ol (MBE) to 2-methylbutan-2-ol (MBA, Scheme 4) at 40 °C in ethanol. Pd is known for high catalytic activity in this reaction, while Ru at the same conditions is not active, both in the presence and absence of a stabilizer. Single atoms of Pd (not ensembles) are known as active sites in this reaction,[36,42] and because the stabilizer (PVP) and its amount (20/1 molar ratio to the metal) is the same for all the catalysts studied, the Ru, Pd, and Ru−Pd systems could be compared in terms of the exposed Pd atoms in the outermost shell of the bimetallic materials. Note that because the stabilizer may affect the catalytic performance, we do not report the turnover frequencies; instead we discuss a qualitative trend based on the observed hydrogenation rates.

Three-phase hydrogenations are well-known for their high susceptibility to mass transfer limitations. The absence of gas−liquid and liquid−solid mass transfer limitations was previously verified by our group for the chosen conditions.[36] In the first step of this investigation, three-phase hydrogenation of MBE to MBA was tested over monometallic Pd and Ru nanoparticles. Pd is extremely active (2.7 $mol_{H2}/(mol_{Pd}\ s)$, while Ru shows no activity. Thus, MBE hydrogenation can be regarded as an effective chemical probe for surface Pd presence in the Ru−Pd bimetallic surfaces.

The MBE hydrogenation rates were determined at 10% MBE conversion and presented in Figure 2 as calculated per total

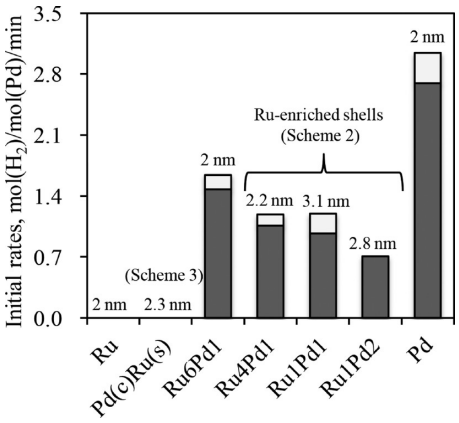

Figure 2. MBE hydrogenation reaction rate per Pd atoms in the bimetallic Ru−Pd catalysts (refer to Scheme 4). The light gray rectangles correspond to one standard deviation.

moles of Pd. The Pd(c)Ru(s) catalyst displays zero activity, confirming the coverage of Pd atoms with an inactive Ru shell. Other Pd−Ru compositions show intermediate activities between Pd and Ru even at the same nanoparticle size (such as 2.0−2.2 nm for Ru6Pd1, Ru4Pd1, and monoPd), indicating the presence of both atoms on the nanoparticle surface. If monometallic Pd and Ru particles were formed instead of the bimetallics, the rates would be the same for Ru6Pd1, Ru4Pd1, and mono-Pd, since the nanoparticle sizes are similar. The fact that Ru4Pd1, Ru1Pd1, and Ru1Pd2 catalysts display lower activity than Ru6Pd1 is consistent with their proposed structure as per the synthesis method (Scheme 2), which allows for the formation of the Ru-enriched shell. Thus, although the bulk Pd content is the lowest in the Ru6Pd1 catalyst, the proportion of Pd in the outermost atomic layer is higher than in the Ru-enriched shell of Ru4Pd1, Ru1Pd1, and Ru1Pd2, which increases its activity. Some differences in the activities of Ru4Pd1, Ru1Pd1, and Ru1Pd2 catalysts may be attributed to the size effect and the reaction's structure-sensitivity.[36] The MBE hydrogenation was shown to proceed on (111) and (100) terraces of Pd nanoparticles with different turnover frequencies.[36] We believe that the three latter catalysts possess different relative amounts of the Pd atoms on these surfaces, which contributes to the activity differences. However, all the three catalysts display the lowest activity (after the monoRu and Pd(c)Ru(s) particles), indicating their surface enrichment with Ru. Thus, the chemical probe results are consistent with the proposed bimetallic structures of the as-synthesized nanoparticles as per their synthetic methods (see Table 1, Schemes 2 and 3).

Catalyst Characterization after High-Temperature Treatment. The as-deposited catalysts were subject to high-temperature treatments in air (up to 400 °C) and hydrogen (375 °C) with the purpose of PVP removal (its decomposition temperature is 350 °C) and as preparation for the indan RO reaction that occurs in the gas phase at 350 °C. As ruthenium

dx.doi.org/10.1021/cs400986v | ACS Catal. 2014, 4, 268−279

may form volatile oxides, NAA of the monometallic Ru and bimetallic Ru4Pd1 samples was performed after 400 °C calcination and 375 °C reduction. Ru content before and after the treatments was found as 0.27 wt % and 0.28 wt % in the monometallic Ru sample, respectively, and did not change for the bimetallic sample either.

The high-temperature treatments are expected to affect the bimetallic nanoparticle structure and size, altering the Ru-to-Pd ratio in the outermost atomic layers as compared with the freshly prepared nanostructures discussed above. The heat of vaporization of Pd (380 kJ/mol) is lower than the one for Ru (580 kJ/mol), so Pd atoms will tend to migrate to the nanoparticle surface driven by the minimization in the nanoparticle's surface energy. A higher Pd fraction is expected to be in the nanoparticle's shell after the high-temperature treatment, as compared with the as-synthesized nanoparticles. The structural transformations are known to depend on the original nanoparticle size, composition, structure, and temperature. They were shown to become significant at ∼1600 K for Pt−Pd nanoparticles of 3 nm size.[43] In the presence of oxygen, the temperature will be lowered because of the significantly lower melting point of metal oxides.

However, for example, under our pretreatment conditions before the catalytic reaction (200 °C calcination, 375 °C reduction), two Ru1Pd1 composites with the same Ru-to-Pd molar ratios and similar particle size (3.1−3.6 nm) but prepared by two different methods (Et reduction resulting in Ru-enriched shells and EG reduction; see Table 1) showed significantly different activities in the indan RO. The EG-reduced Ru1Pd1 catalyst was an order-of-magnitude less active[31] than the one reduced by Et (see the catalytic results section below), indicating a different Pd-to-Ru ratio in the outermost nanoparticle layer (the RO activity of monoRu is higher than that of monoPd). This suggests that the applied pretreatment temperature does not result in the very same bimetallic structure starting from two different structures but of the same size and Pd-to-Ru molar ratio. In the current work, we did not attempt to study the structural transformation process upon heating. The following physicochemical characterization of the materials was performed after the same treatments, and the results were correlated with the observed catalytic reaction results.

CO-TPD was performed after the polymer removal at 350 °C (decomposition temperature of PVP) in air followed by 375 °C reduction. No peaks were detected either for pure γ-alumina support or for a monometallic Ru catalyst with the absence of CO treatment. Figure 3 shows a series of CO-TPD profiles for the selected catalysts. Two CO desorption peaks from Pd nanoparticles centered at 74 and 174 °C could be assigned to the desorption from different Pd sites and/or bridged and linear CO complexes on the nanoparticle surface. A much higher CO desorption temperature centered at 265 °C with strong intensity was observed for the mono-Ru catalyst.

Both Pd(c)Ru(s) and Ru4Pd1 samples reveal a single CO desorption peak at higher temperatures than those of mono-Ru nanoparticles and no low-temperature peaks characteristic for Pd. As per the synthesis techniques (Schemes 3 and 2, respectively), the nanoparticle shell enrichment with Ru is expected, keeping in mind the possible Pd atoms diffusion to the surface because of the high-temperature treatment. Both profiles show a negligible presence of Pd atoms in the outermost layer. The shifts in the Ru peak to higher temperatures may be attributed to the electronic modifications

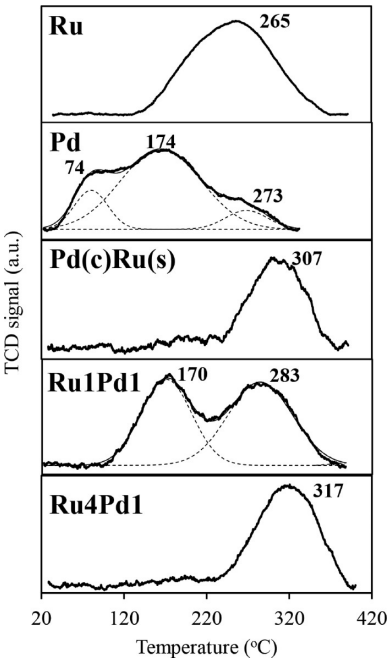

Figure 3. CO-TPD profiles for mono- and bimetallic Ru−Pd catalysts.

on Ru by Pd in bimetallic nanoparticles. Electron affinity of Ru is higher than that of Pd (101 kJ/mol vs 54 kJ/mol), so the electron transfer from Pd to Ru may be expected, resulting in different CO chemisorption strength and further catalytic properties as compared with monometallic Ru.

The CO-TPD profile of the Ru1Pd1 catalyst indicates the significant presence of Pd atoms, but not the monometallic Pd particles, as only one of the Pd peaks is present (170 °C). Note that the catalyst composition (1:1) is close to the Ru/Pd = 1.6 in the Pd(core)-Ru(shell), but after the high-temperature pretreatment, the structures are drastically different (there is negligible Pd in the shell of the core−shell sample), confirming that the molar composition does not control the structure at the applied pretreatment conditions. Less significant shifts in the peaks for the Pd1Ru1 catalyst supports the hypothesis of different loci of Pd and Ru atoms in the selected catalysts. Thus, the CO-TPD results confirm the nanoparticle's bimetallicity and enrichment of the outermost layer of Pd(c)Ru(s) and Ru4Pd1 particles with Ru atoms.

TPR was carried out also after the high-temperature calcination to ensure polymer removal. Pd could be easily reduced and form Pd hydrides below room temperature[44] while the system waits for a stable TCD signal baseline, thus showing only a hydrogen evolution peak centered at 80 °C (see Figure S2 in Supporting Information for the TPR profiles). The reduction of Ru oxide occurs at 85 °C. The Pd−Ru samples showed one peak at the same temperature (80−85 °C). Typically, a conclusion on the nanoparticle's intrinsic bimetallicity is made based on the peak shifts in bimetallic catalysts as compared with the monometallic forms.[20,37,45−47] Because the same peak maxima exist for monometallic Ru and Pd, the TPR was not helpful in elucidating the nanoparticles' structure.

DRIFTS of the adsorbed CO was performed after the pretreatment applied before the catalytic reaction, that is, calcination at 200 °C and reduction at 375 °C. Figure 4 shows the vibrational stretching features of the CO probe in the range of 1850−2200 cm^{-1} frequency (the gas-phase CO band occurs

dx.doi.org/10.1021/cs400986v | ACS Catal. 2014, 4, 268−279

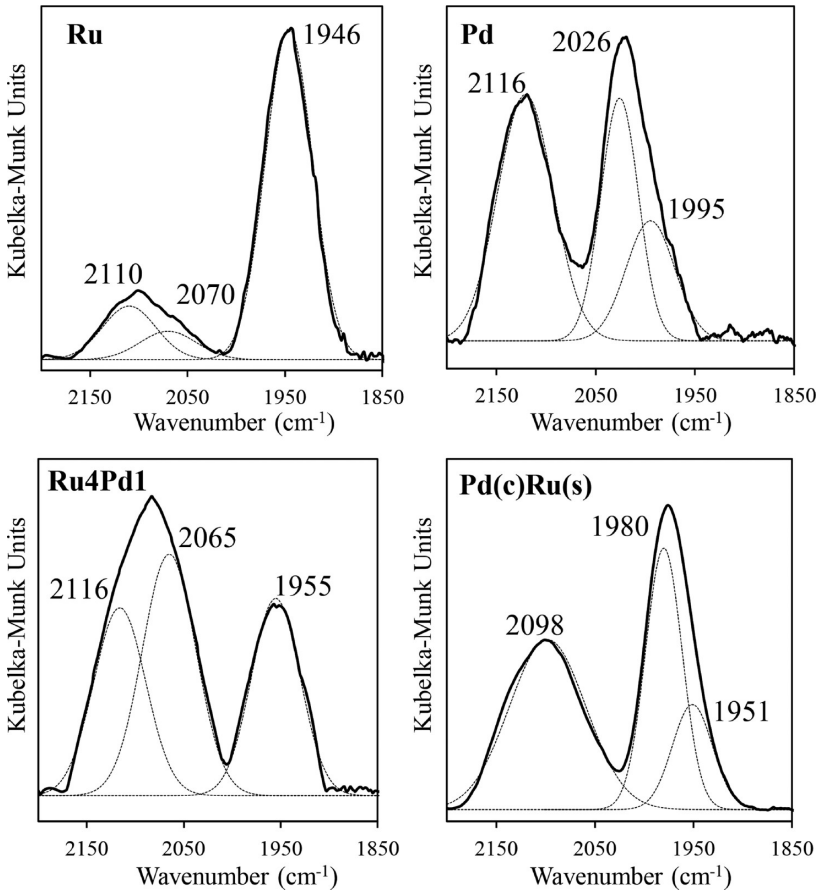

Figure 4. DRIFT spectra of CO adsorbed on mono- and bimetallic Ru−Pd catalysts.

at 2143 cm^{-1}). Two controlled experiments performed on bare alumina support and PVP/alumina showed spectral bands in the frequency below 1700 cm^{-1} that do not interfere with the bands related to the adsorbed CO on the metallic surfaces (2000−2130 cm^{-1} for linear and 1800−2000 cm^{-1} for bridged complexes[46,48,49]). Both Ru and Pd monometallic catalysts display adsorption bands at similar 2110 and 2116 cm^{-1} for the linear mode, with additional 2070 cm^{-1} peak for monoRu, which could be ascribed to the same linear adsorption but on a different surface atom type (i.e., vertex vs terrace). The bridged-adsorbed CO bands occur at 1946 cm^{-1} for Ru and 2026 and 1995 cm^{-1} for Pd. The Pd(c)Ru(s) sample exhibits a peak at 2098 cm^{-1}, which is closer to the linear CO adsorption on monometallic Ru than it is to the one of monoPd, as well as a peak at lower wavenumber. The latter could be deconvoluted into the 1951 cm^{-1} peak characteristic of a bridged CO complex with monometallic-like Ru atoms and a larger-intensity peak at 1980 cm^{-1} that was observed neither for monoPd nor monoRu, and indicates the formation of new CO adsorption sites. These might be either ensembles of Pd and Ru atoms or monoatoms with properties altered by the presence of a second metal; in both instances, this indicates the formation of intrinsic bimetallic nanoparticles. The 2026 and 1995 cm^{-1} peaks for monometallic Pd could not be fitted during the deconvolution. No obvious conclusion on the Ru or Pd enrichment of the surface could be made based only on the DRIFTS of adsorbed CO; however, the CO desorption temperature is indicative of the Ru shell formation, as discussed in the CO-TPD results above.

The Ru4Pd1 spectrum after deconvolution shows peaks at 1955 cm^{-1} (bridged CO adsorption on Ru), 2116 cm^{-1} (linear CO adsorption on either Ru or Pd), and a 2065 cm^{-1} peak that is similar to the linear adsorption on monoRu. These indicate that the Ru4Pd1 surface is mainly governed by Ru presence but at the same time the relative intensities of linear-to-bridged adsorption peaks are much higher for the Ru4Pd1 catalyst than for monoRu, which implies Ru surface dilution with Pd atoms, that is, bimetallicity. The CO desorption temperature was also different as compared with the monometallic catalysts. These results are in line with the applied synthetic procedure: monometallic Ru nanoparticles cannot be formed in ethanol; rather, they can be formed only in combination with Pd present as seeds.

Thus, a combination of the applied characterization techniques after the high-temperature treatment confirmed the intrinsic bimetallicity of the catalysts and indicated the shell enrichment with Ru atoms for Pd(c)Ru(s) and Ru4Pd1 samples.

TEM of supported calcined catalysts was performed to evaluate possible sintering of nanoparticles after the high-temperature treatment. The results may be also indicative of intrinsic bimetallicity because the addition of a second metal often allows for better thermal stabilities of the resulting bimetallic catalysts. An example of the beneficial effect on thermal stability by alloying two metals has been previously reported by Strobel et al.:[44] both pure Pd and Pt sintered to a large extent, while the addition of a very small amount of Pt stabilized the Pd particles and prevented sintering at 800 °C.[44] Figure 5 shows exemplary TEM images of selected catalysts

dx.doi.org/10.1021/cs400986v | ACS Catal. 2014, 4, 268−279

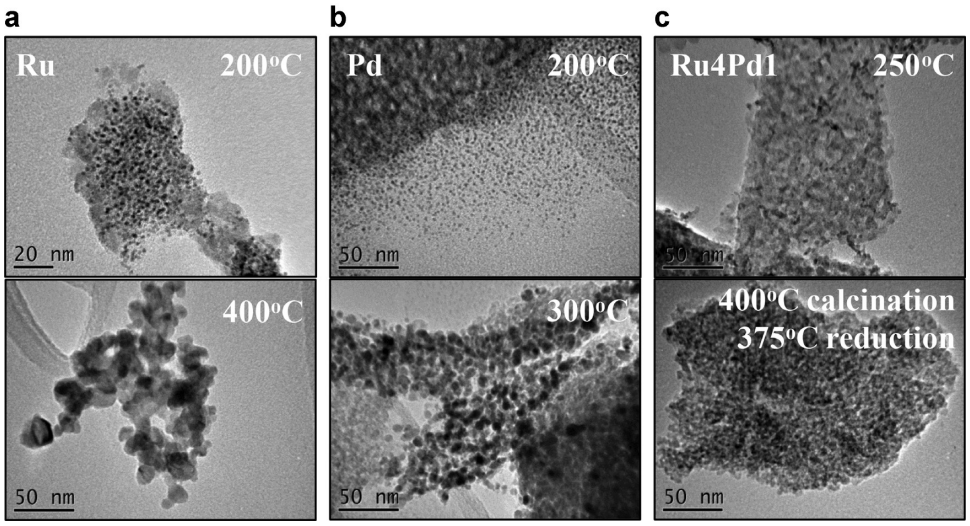

Figure 5. TEM images of Ru/γ-Al_2O_3 (left), Pd/γ-Al_2O_3 (center), and Ru4Pd1/γ-Al_2O_3 (right) catalysts after precalcination in air at different temperatures and reduction in hydrogen at 375 °C.

after calcination. Monometallic Pd and Ru are not resistant to sintering and showed agglomerates in the 300−400 °C range. For the bimetallic sample Ru4Pd1 (this catalyst was found as the most promising in indan RO, as reported below), the nanoparticle sintering did not occur after 400 °C calcination and 375 °C reduction in H_2. This improved thermal stability upon alloying Ru with Pd can be considered as another piece of evidence for intrinsic bimetallicity in Ru4Pd1 sample.

CO Chemisorption. To verify the effect of the calcination treatment on the nanoparticles' agglomeration, CO chemisorption was performed for Ru and Ru4Pd1 catalysts calcined at different temperatures and reduced at 375 °C (Figure 6). CO

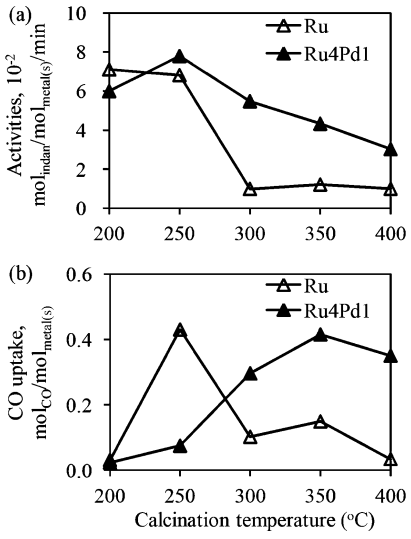

Figure 6. Effect of calcination temperatures on catalytic activities in indan RO (a) and CO uptakes from CO-chemisorption (b).

chemisorption of the alumina support is negligible (<0.1 $\mu mol_{CO}/g_{alumina}$). The obtained CO uptakes were corrected for the support uptake. As expected from the TEM results on the nanoparticles' sintering, for the monoRu, the dispersion drops significantly starting at 300 °C, with maximum dispersion at 250 °C. Ru4Pd1, on the other hand, at 350 and 400 °C showed highest dispersions of ∼40% that corresponds to ∼2.3 nm particles. The dispersion value is obtained assuming 1:1 CO:metal stoichiometry, which overestimates particle size since bridged CO is also present (as evidenced by DRIFTs). Thus, the obtained overestimated value of 2.3 nm confirms the particles' thermal stability, since the original size of the as-synthesized nanoparticles is 2.2 ± 0.5 nm (Table 1). Very low amounts of adsorbed CO after 200 °C calcination for both samples are due to the residuals of PVP, which prevents the CO chemisorption. The XPS analysis of the Ru4Pd1 catalyst after the 200 °C calcination-375 °C reduction treatment showed that the N/Ru molar ratio was reduced from 2.5 (fresh) to 1.1 (calcined), confirming the presence of PVP residuals on the catalyst surface.

However, before concluding on the optimal calcination temperature as one that balances between resistance to sintering and PVP removal efficiency, the catalytic activities must be taken into consideration. For example, Rioux et al. found that the ethylene hydrogenation activity on PVP-stabilized Pt-nanoparticles was maximized with an in situ oxidation−reduction cycle at 200 °C.[50] The indan RO activity was evaluated as a function of the catalyst pretreatment conditions (Figure 6). As seen, the amount of the adsorbed CO is not indicative of the most optimal pretreatment temperature and does not correlate with the RO activity trends. The reasons of such behavior are under investigation and will be reported separately. The RO activity of Ru4Pd1 catalyst was maximized at 200−250 °C calcination. Combining the CO-chemisorption and TEM results, as well as the indan RO activities, the mono- and bimetallic Ru−Pd catalysts to be used for the indan RO reaction should be calcined at a temperature not higher than 250 °C.

Catalytic Behavior in RO. Table 2 and Figure 7 compare activities and selectivities in indan RO for the developed catalysts. Ir is the most active catalyst, and Ru shows one-fourth of the activity of Ir in indan RO, whereas Pd and Pt reveal the lowest activities, which are the expected trends for these metals. Iridium also results in the lowest lights formation among all monometallic catalysts. Pt allows the highest ratio of *n*-propylbenzene to 2-ethyltoluene, which is in agreement with a known adsorbed flat-lying olefin mechanism for Pt. Pt results in the highest toluene (57%) and lights formation, which is a

dx.doi.org/10.1021/cs400986v | ACS Catal. 2014, 4, 268−279

Table 2. Catalytic Activities and Product Selectivities in Indan RO

			selectivities, %						
catalyst	conversion, %	activity, 10^{-2} $mol_{indan}/mol_{metal(s)}$·min	2-ethyl-toluene	*n*-propyl-benzene	ethyl-benzene	*o*-xylene	benzene	toluene	lights
Ru[a]	37	4 (0)	17 (0)	2 (0)	2(0)	40 (3)	2 (0)	16 (0)	21 (3)
Pd[b]	8	1 (0)	73 (-)	10 (-)	1(-)	2 (-)	2 (-)	8 (-)	5 (-)
Ir[c]	46	16 (4)	62 (5)	3 (0)	1(0)	22 (0)	1 (0)	5 (0)	6 (1)
Pt[d]	1	1 (-)	8 (-)	13 (-)	1(-)	1 (-)	7 (-)	57 (-)	13 (-)
Ru10Pd1[a]	41	5 (0)	26 (2)	2 (0)	3(0)	34 (1)	2 (0)	16 (0)	18 (1)
Ru8Pd1[d]	20	2 (0)	37 (4)	2 (0)	2(0)	29 (2)	2 (0)	14 (1)	14 (1)
Ru6Pd1[d]	17	2 (-)	44 (-)	2 (-)	2(-)	25 (-)	1 (-)	12 (-)	13 (-)
Ru4Pd1[d]	27	4 (0)	59 (6)	4 (0)	2(1)	21 (2)	1 (1)	2 (1)	7 (2)
Ru2Pd1[d]	19	3 (-)	60 (-)	4 (-)	1(-)	20 (-)	2 (-)	8 (-)	7 (-)
Ru1Pd1[d]	8	1 (0)	50 (7)	5 (2)	1(0)	16 (2)	7 (3)	13 (4)	8 (0)
Ru1Pd2[d]	5	1 (-)	52 (-)	5 (-)	1(-)	13 (-)	9 (-)	13 (-)	8 (-)
Pd(c)Ru(s)[a]	33	5 (1)	44 (3)	3 (0)	2(0)	31 (3)	1 (0)	9 (1)	9 (0)

[a]2 mg of active metal(s). [b]9 mg of active metal. [c]1 mg of active metal. [d]4 mg of active metals. Data in brackets correspond to one standard deviation.

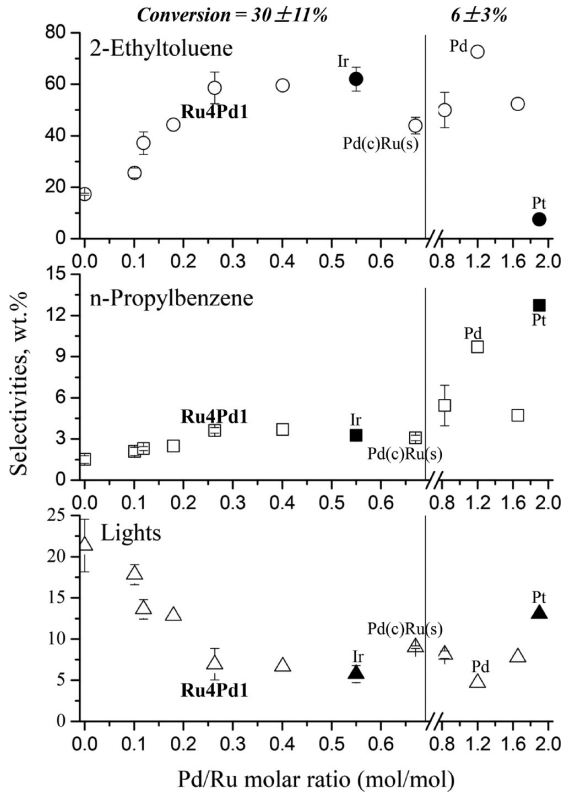

Figure 7. Selectivities vs Pd-to-Ru molar ratio in the bimetallic and monometallic catalysts (monometallic Ir and Pt catalysts are included for comparison). The catalysts were grouped according to similar indan conversions for fair selectivity comparison.

drawback in terms of single cleavage products. Pd displays poor RO activity but the highest single cleavage selectivity (sum of 2-ethyltoluene and *n*-propylbenzene selectivities) at this low conversion. Monometallic Ru favors deep hydrogenolysis, resulting in high *o*-xylene (40%) and lights formation (21%).

When Pd is added to Ru, it tempers its undesirable hydrogenolysis activity with a simultaneous decrease in activity. Figure 7 is plotted in terms of the Pd-to-Ru molar ratio in the catalysts and is grouped into two regions of conversion range, as the high Pd amount results in low conversion, which does not allow for direct selectivity comparison at higher conversions for high Ru amount. Between 0 and 0.25 Pd-to-Ru ratio, the selectivity to 2-ethyltoluene improves 3-fold with corresponding 3-fold suppression in lights formation, reaching the values for monometallic Ir. With the further ratio increase, no further selectivity improvement is observed; it is undesirable from the viewpoint of activity. It is important to note that the bimetallic nanoparticle structure control is paramount: the Pd(core)-Ru(shell) catalyst falls off the trend because of the abundance of Ru atoms despite of high bulk Pd-to-Ru ratio. Its activities and selectivities approach the values for the Ru10Pd1−Ru6Pd1 systems, confirming the shell enrichment with Ru.

The incorporation of Pd to the Ru catalyst improved the selectivity to *n*-propylbenzene 2-fold and reached the level for Ir (Figure 7). The monometallic Pt catalyst gives the highest selectivity to *n*-propylbenzene because of a different RO mechanism via the olefin flat-lying model; on the other hand, it promotes lights production and, thus, it underperforms the Ru4Pd1 catalysts at preserving the molecular weight of the cleaved indan.

Ruthenium, similar to Ir, exhibits a dicarbene path in RO, which requires perpendicular adsorption of a reactant on two metal atoms.[1,18] Pd works through a flat-lying π-adsorbed olefin mode (with low activity); thus, its addition to Ru may dilute the Ru ensembles, decreasing the activity. On the other hand, the formed single cleavage products may adsorb on the Pd atoms in Ru−Pd systems via the π- olefin mode, which prevents their further dealkylation to *o*-xylene and toluene, characteristic for mono Ru. This results in the improved selectivity. The electronic effects due to the different electronic affinities may be also responsible for the observed synergism.

Thus, the most optimal Pd−Ru composition corresponding to the highest selectivity toward single cleavage at the minimal loss of activity is the Ru4Pd1 catalyst: its selectivities are either equal or outperform the monometallic Ir and Pt selectivities, which makes the Ru−Pd system a valid alternative to Ir for the RO reactions. The conclusion should not be extrapolated to any Ru−Pd systems with similar 4:1 molar ratios of metals because of the residuals of PVP adsorbed on the reported system, which may affect the catalytic behavior. According to the XPS analysis of the Ru4Pd1 catalyst, the N/Ru molar ratio dropped from 2.5 to 1.1 after the 200 °C calcination and 375 °C reduction, as used before the catalytic runs. The Cl/Ru ratio decreased from 0.3 to 0.2 after the treatment. The current study shows the possibility of avoiding rare and expensive Ir by

dx.doi.org/10.1021/cs400986v | ACS Catal. 2014, 4, 268−279

introducing a more available and less expensive alternative bimetallic system that allows the same RO selectivity as Ir.

CONCLUSIONS

Bimetallic Pd−Ru nanoparticles of ∼2−3 nm size with varying molar ratio of Pd-to-Ru from 0 to 1.7 were synthesized in the presence of PVP, deposited on alumina and tested in the indan RO at atmospheric pressure. The synthetic methods allowed for preparing the nanoparticles with Ru abundance in the nanoparticle shell. The intrinsic bimetallic nature of the nanoparticles was consistent with the results of CO-TPD, CO-DRIFTS, thermal stability tests, and a chemical probe reaction (olefin hydrogenation with only Pd atoms active). TEM revealed nanoparticle monodispersity, which was maintained after the high-temperature PVP removal for bimetallic systems, with pronounced sintering in the case of monoforms. A study of the PVP removal at different calcination temperatures, performed by comparing the RO activities with the metallic surface available for CO chemisorption, showed that the amount of the adsorbed CO is not indicative of the most optimal pretreatment temperature found as 200−250 °C for the maximized catalytic activity.

The catalytic tests of indan RO showed the dramatic 3-fold increase in the selectivity to 2-ethyltoluene when the Pd-to-Ru molar ratio increased from 0 to 0.25, with no further improvement in selectivity and loss of activity because of the high proportion of low-active Pd. The Ru4Pd1 catalyst displayed the same high single cleavage selectivity and as low lights formation as iridium, which is known as the most selective RO metal.

ASSOCIATED CONTENT

Supporting Information

TEM images and size distribution histograms of PVP-stabilized bimetallic Ru−Pd colloids and TPR profiles of Ru, Ru4Pd1, Ru1Pd1 and Pd catalysts. This material is available free of charge via the Internet at http://pubs.acs.org.

AUTHOR INFORMATION

Corresponding Author

*E-mail: semagina@ualberta.ca. Phone: 1-780-492-2293. Fax: 1-780-492-2881.

Notes

The authors declare no competing financial interest.

ACKNOWLEDGMENTS

We thank the Centre for Oil Sands Innovation at the University of Alberta and Canada Foundation for Innovation (New Leaders Opportunities) for financial support, Dr. Mainak Ghosh (Imperial Oil Resources, Calgary, Canada) for fruitful discussions, Dr. Dimitre Karpuzov (U of A) for XPS measurements, Dr. J. Duke (U of A) and Becquerel Laboratory (Ontario, Canada) for the NAA analyses.

REFERENCES

(1) McVicker, G. B.; Daage, M.; Touvelle, M. S.; Hudson, C. W.; Klein, D. P.; W. C., B., Jr.; Cook, B. R.; Chen, J. G.; Hantzer, S.; Vaughan, D. E. W.; Ellis, E. S.; Feeley, O. C. *J. Catal.* **2002**, *210*, 137−148.
(2) Santana, R. C.; Do, P. T.; Santikunaporn, M.; Alvarez, W. E.; Taylor, J. D.; Sughrue, E. L.; Resasco, D. E. *Fuel* **2006**, *85*, 643−656.
(3) Du, H.; Craig, F.; Yang, H.; Zbigniew, R. *Appl. Catal., A* **2005**, *294*, 1−21.
(4) Do, P. T.; Alvarez, W. E.; Resasco, D. E. *J. Catal.* **2006**, *238*, 477−488.
(5) Moraes, R.; Thomas, K.; Thomas, S.; van Donk, S.; Grasso, G.; Gilson, J. P.; Houalla, M. *J. Catal.* **2012**, *286*, 62−77.
(6) Dokjampa, S.; Rirksomboon, T.; Osuwan, S.; Jongpatiwut, S.; Resasco, D. E. *Catal. Today* **2007**, *123*, 218−223.
(7) Blackmond, D. G.; Goodwin, J. G.; Lester, J. E. *J. Catal.* **1982**, *78*, 34−43.
(8) Kubicka, D.; Kumar, N.; Maki-Arvela, P.; Tiitta, M.; Niemi, V.; Karhu, H.; Salmi, T.; Murzin, D. Y. *J. Catal.* **2004**, *227*, 313−327.
(9) Marcilly, C. *J. Catal.* **2003**, *216*, 47−62.
(10) Santikunaporn, M.; Herrera, J. E.; Jongpatiwut, S.; Resasco, D. E. *J. Catal.* **2004**, *228*, 100−113.
(11) Kubicka, D.; Kangas, M.; Kumar, N.; Tiitta, M.; Lindblad, M.; Murzin, D. Y. *Top. Catal.* **2010**, *53*, 1438−1445.
(12) Gault, F. G. *Adv. Catal.* **1981**, *30*, 1.
(13) Piegsa, A.; Korth, W.; Demir, F.; Jess, A. *Catal. Lett.* **2012**, *142*, 531−540.
(14) Lecarpentier, S.; Gestel, v.; G., J.; Thomas, K.; Gilson, J. P.; Houalla, M. *J. Catal.* **2008**, *254*, 49−63.
(15) Sinfelt, J. H.; Heights, B. U.S. Patent 3,953,368, 1976.
(16) Djeddi, A.; Fechete, I.; Garin, F. *Appl. Catal., A* **2012**, *413−414*, 340−349.
(17) Zhao, Z. J.; Moskaleva, L. V.; Rösch, N. *ACS Catal.* **2013**, *3*, 196−205.
(18) Samoila, P.; Boutzeloit, M.; Especel, C.; Epron, F.; Marécot, P. *Appl. Catal., A* **2009**, *369*, 104−112.
(19) Coq, B.; Figueras, F. *J. Mol. Catal. A* **2001**, *173*, 117−134.
(20) Samoila, P.; Boutzeloit, M.; Especel, C.; Epron, F.; Marécot, P. *J. Catal.* **2010**, *276*, 237−248.
(21) Poupin, C.; Pirault-Roy, L.; La Fontaine, C.; Tóth, L.; Chamam, M.; Wootsch, A.; Paál, Z. *J. Catal.* **2010**, *272*, 315−319.
(22) Espinosa, G.; Del Angel, G.; Barbier, J.; Bosch, P.; Lara, V.; Acosta, D. *J. Mol. Catal. A* **2000**, *164*, 253−262.
(23) Teschner, D.; Pirault-Roy, L.; Naudb, D.; Guérin, M.; Paál, Z. *Appl. Catal., A* **2003**, *252*, 421−426.
(24) Ziaei-azad, H.; Yin, C. X.; Shen, J.; Hu, Y.; Karpuzov, D.; Semagina, N. *J. Catal.* **2013**, *300*, 113−124.
(25) Piccolo, L.; Nassreddine, S.; Aouine, M.; Ulhaq, C.; Geantet, C. *J. Catal.* **2012**, *292*, 173−180.
(26) Xu, F.; Bauer, L. J.; Gillespie, R. D.; Bricker, M. L.; Bradley, S. A. U.S. Patent WO/2007/041605, 2007.
(27) Le Normand, F.; Kili, k.; Schmitt, J. L. *J. Catal.* **1993**, *139*, 234−255.
(28) Gaspar, A. B.; Dieguez, L. C. *Appl. Catal., A* **2000**, *201*, 241−251.
(29) Del Angel, G.; Coq, B.; Dutartre, R.; Figueras, F. *J. Catal.* **1984**, *87*, 27−35.
(30) Pan, C.; Dassenoy, F.; Casanove, M. J.; Philippot, K.; Amiens, C.; Lecante, P.; Mosset, A.; Chaudret, B. *J. Phys. Chem. B* **1999**, *103*, 10098−10101.
(31) Shen, J.; Yin, X.; Karpuzov, D.; Semagina, N. *Catal. Sci. Technol.* **2013**, *3*, 208−221.
(32) Teranishi, T.; Miyake, M. *Chem. Mater.* **1998**, *10*, 594−600.
(33) Chen, Y.; Liew, K. Y.; Li, J. *Mater. Lett.* **2008**, *62*, 1018−1021.
(34) Borodko, Y.; Habas, S. E.; Koebel, M.; Yang, P.; Frei, H.; Somorjai, G. A. *J. Phys. Chem. B* **2006**, *110*, 23052−23059.
(35) Liu, M.; Zhang, J.; Liu, J.; Yu, W. W. *J. Catal.* **2011**, *278*, 1−7.
(36) Ma, R.; Semagina, N. *J. Phys. Chem. C* **2010**, *114*, 15417−15423.
(37) Nylén, U.; Sassu, L.; Melis, S.; Järås, S.; Boutonnet, M. *Appl. Catal., A* **2006**, *299*, 1−13.
(38) Li, Y.; Boone, E.; El-Sayed, M. A. *Langmuir* **2002**, *18*, 4921−4925.
(39) Corain, B., Schmid, G., Toshima, N., Eds.; In *Metal nanoclusters in catalysis and materials science: the issue of size control*; Elsevier: Amsterdam, The Netherlands, 2007; p 470.
(40) Ciacchi, L. C.; Pompe, W.; De Vita, A. *J. Phys. Chem. B* **2003**, *107*, 1755−1764.
(41) van Hardeveld, R.; Hartog, F. *Surf. Sci.* **1969**, *15*, 189−230.

(42) Crespo-Quesada, M.; Yarulin, A.; Jin, M.; Xia, Y.; Kiwi-Minsker, L. *J. Am. Chem. Soc.* **2011**, *133*, 12787−12794.
(43) Huang, R.; Wen, Y.-H.; Zhu, Z.-Z.; Sun, S.-G. *J. Phys. Chem. C* **2012**, *116*, 8664−8671.
(44) Strobel, R.; Grunwaldt, J. D.; Camenzind, A.; Pratsinis, S. E.; Baiker, A. *Catal. Lett.* **2005**, *104*, 9−16.
(45) Dokjampa, S.; Rirksomboon, T.; Phuong, D. T. M.; Resasco, D. E. *J. Mol. Catal. A* **2007**, *274*, 231−240.
(46) Niemantsverdriet, J. W., Ed.; In *Spectroscopy in Catalysis*; Wiley-VCH: Weinheim, Germany, 2007.
(47) Nylen, U.; Pawelec, B.; Boutonnet, M.; Fierro, J. L. G. *Appl. Catal., A* **2006**, *299*, 14−29.
(48) Kappers, M.; Dossi, C.; Psaro, R.; Recchia, S.; Fusi, A. *Catal. Lett.* **1996**, *39*, 183−189.
(49) Riguetto, B. A.; Bueno, J. M. C.; Petrov, L.; Marques, C. M. P. *Spectrochimica Acta, Part A* **2003**, *59*, 2141−2150.
(50) Rioux, R. M.; Song, H.; Grass, M.; Habas, S.; Niesz, K.; Hoefelmeyer, J. D.; Yang, P.; Somorjai, G. A. *Top. Catal.* **2006**, *39*, 167−174.